European Journal of Pharmaceutical Sciences 184 (2023) 106421

Contents lists available at ScienceDirect

European Journal of Pharmaceutical Sciences

journal homepage: www.elsevier.com/locate/ejps

Evaluation of the ^{18}F-labeled analog of the therapeutic all-D-enantiomeric peptide RD2 for amyloid β imaging

Antje Willuweit [a,*], Swen Humpert [a], Michael Schöneck [a], Heike Endepols [a,b,c], Nicole Burda [a], Lothar Gremer [d,e], Ian Gering [d], Janine Kutzsche [d], N.Jon Shah [a,f,g], Karl-Josef Langen [a,h], Bernd Neumaier [a,b], Dieter Willbold [d,e], Alexander Drzezga [a,c]

[a] Institute of Neuroscience and Medicine-4 (INM-2, INM-4, INM-5, INM-11), Forschungszentrum Jülich, Jülich 52425, Germany
[b] Institute of Radiochemistry and Experimental Molecular Imaging, Faculty of Medicine and University Hospital Cologne, University of Cologne, Cologne 50937, Germany
[c] Department of Nuclear Medicine, Faculty of Medicine and University Hospital Cologne, University of Cologne, Cologne 50937, Germany
[d] Institute of Biological Information Processing (IBI-7), Forschungszentrum Jülich, Jülich 52425, Germany
[e] Institut für Physikalische Biologie, Heinrich-Heine-Universität Düsseldorf, Düsseldorf 40225, Germany
[f] JARA - Brain - Translational Medicine, Aachen 52074, Germany
[g] Department of Neurology, RWTH Aachen University, Aachen 52074, Germany
[h] Department of Nuclear Medicine, RWTH Aachen University, Aachen 52074, Germany

ARTICLE INFO

Keywords:
Pet probe
Amyloid beta oligomers
Ad mouse model
Preclinical
D-enantiomeric peptide
Radioligand

ABSTRACT

Positron emission tomography (PET) imaging with radiotracers that bind to fibrillary amyloid β (Aβ) deposits is an important tool for the diagnosis of Alzheimer's disease (AD) and for the recruitment of patients into clinical trials. However, it has been suggested that rather than the fibrillary Aβ deposits, it is smaller, soluble Aβ aggregates that exert a neurotoxic effect and trigger AD pathogenesis. The aim of the current study is to develop a PET probe that is capable of detecting small aggregates and soluble Aβ oligomers for improved diagnosis and therapy monitoring. An ^{18}F-labeled radioligand was prepared based on the Aβ-binding D-enantiomeric peptide RD2, which is currently being evaluated in clinical trials as a therapeutic agent to dissolve Aβ oligomers. ^{18}F-labeling was carried out using palladium-catalyzed S-arylation of RD2 with 2-[^{18}F]fluoro-5-iodopyridine ([^{18}F]FIPy). Specific binding of [^{18}F]RD2-cFPy to brain material from transgenic AD (APP/PS1) mice and AD patients was demonstrated with *in vitro* autoradiography. *In vivo* uptake and biodistribution of [^{18}F]RD2-cFPy were evaluated using PET analyses in wild-type and transgenic APP/PS1 mice. Although brain penetration and brain wash-out kinetics of the radioligand were low, this study provides proof of principle for a PET probe based on a D-enantiomeric peptide binding to soluble Aβ species.

1. Introduction

Amyloid β (Aβ) peptides play a central role in the pathogenesis of Alzheimer's disease (AD). Released by proteolytic cleavage from the amyloid precursor protein (APP), monomeric Aβ eventually assembles into oligomeric forms, which can act as seeds for further growth into protofibrils and fibrils. These high molecular weight assemblies are deposited as amyloid plaques in the brains of AD patients. Contrary to previous assumptions, it is now suggested that soluble Aβ oligomers, rather than fibrils, are the most toxic species causing neurodegeneration in AD (Walsh and Selkoe, 2007). These Aβ oligomers even possess some properties of prions, *e.g.* the propagation between different brain areas and the existence of various polymorphisms or strains based on different conformations (LeVine and Walker, 2016; Willbold et al., 2021).

Various Aβ based biomarkers have been developed in recent years, including Aβ levels in body fluids and radiotracers for positron emission tomography (PET) to quantify amyloid load in the brain. The ^{11}C-labeled Pittsburgh Compound B (PiB) was the first broadly applied radiotracer specifically detecting Aβ in the living human brain. PiB has been shown to possess high affinity and selectivity to fibrillar Aβ in

Abbreviation: AD, Alzheimer's disease; Aβ, amyloid β; APP, amyloid precursor protein; IV, intravenous; PET, positron emission tomography; p.i., post injection; PiB, Pittsburgh Compound B; RCYs, radiochemical yields; VOI, volume of interest.

* Corresponding author.
E-mail address: a.willuweit@fz-juelich.de (A. Willuweit).

https://doi.org/10.1016/j.ejps.2023.106421
Received 30 September 2022; Received in revised form 16 February 2023; Accepted 5 March 2023
Available online 6 March 2023

plaques and other Aβ containing lesions (Cohen et al., 2012). However, due to the short half-life of the ^{11}C radioisotope (20 min), ^{18}F-labeled compounds such as Florbetapir, Florbetaben, and Flutemetamol have been developed. The longer half-life of ^{18}F (110 min) confers logistical advantages as it allows transportation of the radiotracers to more distant PET centers. All three ^{18}F-labeled PET-tracers mentioned above possess specific amyloid binding and show robust differences in tracer retention between patients with AD and age-matched controls (Rowe et al., 2008; Wong et al., 2010; Serdons et al., 2009). In contrast to Aβ biomarkers in bodily fluids, amyloid PET can also provide information about the localization and spread of amyloid pathology in the brain (Villain et al., 2012). Longitudinal studies using amyloid PET imaging have clearly demonstrated the temporal relationships between the manifestation of amyloid deposits and the development of later disease stages (Roberts et al., 2018; Jack et al., 2013). Despite this, tracer uptake is poorly correlated to the severity of symptoms and tends to plateau in the later stages of the disease (Jack et al., 2013; Mallik et al., 2017). Genetic and clinical evidence points to a stronger association of Aβ oligomers, rather than fibrillary plaques, with the development of AD. Rare APP mutations leading to early onset AD, *i.e.*, Osaka (E22D) and Arctic (E22G) mutations, result in increased cerebral levels of soluble Aβ species but minimal fibrillary amyloid deposits, as confirmed by very low signals in amyloid PET scans (Scholl et al., 2012; Tomiyama et al., 2008). In addition, the effectiveness of anti-amyloid therapies in recent clinical trials mirrored the agents' various degrees of selectivity towards Aβ oligomers (Tolar et al., 2021). In this context, PET tracers that recognize all aggregated Aβ assemblies, *i.e.*, Aβ fibrils and soluble oligomeric forms, would be of clinical value to aid diagnosis in patients devoid of fibrillary Aβ.

In recent years, we have developed D-enantiomeric peptides that destabilize and disassemble Aβ oligomers and other Aβ assemblies as a therapeutic strategy against AD. The lead compound, D3, was discovered through mirror image phage display and was found to be effective in mouse models of AD by reducing cerebral Aβ aggregates and reversing cognitive deficits (Funke and Willbold, 2009; Aileen Funke et al., 2010; van Groen et al., 2013). Further optimization of the compound led to RD2, a clinical-stage derivative (Kutzsche et al., 2020), the efficacy of which has been proven in several preclinical proof-of-concept studies in transgenic mouse models of AD (van Groen et al., 2017; Kutzsche et al., 2017; Schemmert et al., 2019a, 2019b) and old beagle dogs (Kutzsche et al., unpublished results). RD2 binds with nanomolar affinity to Aβ monomers, including Aβ subunits in oligomers and larger aggregates (Zhang et al., 2019). No significant binding to other amyloidogenic proteins, such as tau or α-synuclein, has been found ($K_D \geq 1$ mM, Kutzsche, personal communication). The binding of RD2 to Aβ subunits leads to the disassembly of the Aβ complexes, as demonstrated *in vitro* (van Groen et al., 2017), *in vivo* (Schemmert et al., 2019b), and recently also *ex vivo* with patient-derived brain material (Kass et al., 2022). RD2 is an all-D-peptide consisting of only D-enantiomeric amino acid residues. All-D-peptides are known to be non-immunogenic (Wiesehan and Willbold, 2003) and, due to their protease resistance, are very stable in bodily fluids (Elfgen et al., 2019, 2017).

The aim of the current study is to explore the potential of RD2 for the development of a PET probe able to recognize Aβ assemblies of various sizes and structures. Given its unique binding mode to monomeric Aβ subunits of aggregates, an RD2-based radioligand was expected to bind to all species of Aβ assemblies irrespective of size or polymorphic conformation, including fibrillary and oligomeric Aβ. Here, we designed and evaluated an ^{18}F-labeled RD2 PET probe and demonstrated specific binding to brain material from transgenic AD mice and AD patients. The biodistribution of [^{18}F]RD2-cFPy was shown in wild-type and transgenic mice via PET analyses, providing *in vivo* proof of concept for a PET probe based on a D-enantiomeric peptide.

2. Materials and methods

2.1. Peptides

The all-D-enantiomeric peptide RD2 (consisting of 12 D-enantiomeric amino acid residues and amidated C-terminus) (H-ptlhthnrrrrr-NH2, 1598.8 Da, purity ≥98.2%) was produced by CBL Patras (Patras, Greece). RD2 containing an additional D-cysteine at the C-terminus (RD2cys, H-ptlhthnrrrrr-c-NH2, 1702.0 Da, purity ≥95.7%) for subsequent in-house fluorescence labeling was custom-synthesized by Peptides and Elephants (Henningsdorf, Germany). The purity, identity, and chirality of the peptides were confirmed by RP-HPLC, mass spectroscopy, and CD spectroscopy, respectively.

2.2. Animals

All animal experiments were performed in accordance with the German law on the protection of animals (TierSchG §§ 7–9) and were approved by the local ethics committee (Landesamt für Natur, Umwelt und Verbraucherschutz Nordrhein-Westfalen (LANUV), North-Rhine-Westphalia, Germany, Az 84–02.04.2014.A362, Az 84–02.04.2017.A029 and Az 81–02.04.2019.A304).

For PET analysis, fluorescence staining, and *in vitro* autoradiography, animals from the following transgenic APP/PS1 mouse line were used:

Homozygous ARTE10 mice (B6.Cg-Tg(Thy1-PSEN1*M146V/Thy1-APP*swe)−10Arte) expressing APPswe and PS1-M146V under Thy1.1 regulatory sequences were a generous gift from Taconic Biosciences, Inc. (Germantown, NY, USA). Mice develop a progressive AD-like amyloid pathology with abundant deposits throughout the whole brain, with the exception of the cerebellum (Willuweit et al., 2009). Five 24-month-old homozygous ARTE10 animals (three females and two males) were used for this study. Six aged-matched C57Bl/6 J mice (two females and four males), bred in-house, served as control animals.

All mice were kept in a controlled environment, with a 24 h light/dark cycle (12/12 h), 54% humidity, and a temperature of 22 °C. Food and water were available *ad libitum*.

2.3. Human brain material

Frozen samples of postmortem brain tissue from human AD patients and age-matched controls were obtained from the Netherlands Brain Bank (NBB, Amsterdam, The Netherlands) following approval of the ethics committee at Heinrich Heine University Düsseldorf (Germany, study ID: 2018–115-FmB). The Netherlands Brain Bank adheres to strict ethical guidelines, as stated in BrainNet Europe's Ethical Code of Conduct for brain banking, and holds ethical approval from the University Medical Center of Amsterdam, The Netherlands. Clinicopathological diagnosis was performed based on the criteria of probable AD (McKhann et al., 1984; Dubois et al., 2007) and was confirmed by neuropathological analysis of the autopsy. Frozen samples from the cortical superior occipital gyrus of a male diagnosed with AD and congophilic angiopathy (Braak stage 4, 87 years old) and from the cerebellum of a female non-demented control Braak stage 0, 64 years old) were included in this study.

2.4. Tissue collection and cryo sectioning

Mice were killed by cervical dislocation, and the brains were excised immediately. The brains were divided into the two hemispheres, snap frozen in -50 °C isopentane, and stored at −80 °C until further use. Frozen mouse and human brain samples were cut into 20 μm sections using a cryostat (Leica CM 3050 S, Leica Microsystems, Wetzlar, Germany) and stored at −80 °C.

2.5. Fluorescence labeling of peptides

ATTO488 fluorescence labeled RD2, termed RD2-c488, was synthesized by reacting RD2cys with a threefold molar excess of ATTO488-maleimide (MW 1067 g mol^{-1}, ATTO-TEC, Siegen, Germany), leading to covalent attachment of the ATTO488 fluorophor to the C-terminal D-cysteine residue of RD2cys.

Typically, 1 mg of ATTO488-maleimide dye (0.94 μmol) was freshly dissolved in 100 μl N,N-dimethylformamide (DMF), then a 900 μl 200 mM HEPES/NaOH buffer, pH 7.6 was added, and the dissolved dye was applied to 5 mg (2.94 μmol) RD2cys. After incubation for 1−2 h at RT, the reaction mixture was applied to a semipreparative RP-HPLC on a C8 column (Agilent Zorbax-300 SB, 9.4 mm × 250 mm column dimension, consecutive injections of ~300 μl sample aliquots) connected to an Agilent 1260 HPLC system (Agilent, Germany). The purification of RD2-c488 was achieved by applying an aqueous acetonitrile (ACN) gradient (7.5% ACN, 0.1% trifluoroacetic acid (TFA) to 30% ACN, 0.1% TFA in Milli-Q water within 30 min), running at a flow rate of 4 ml min^{-1} at 25 °C with ultraviolet and visible absorbance detection at 214 and 503 nm, respectively. The purified RD2-c488 samples (purity >98%) were collected, aliquoted, flash-frozen in liquid N_2, and freeze-dried *in vacuo* (LT-105, Martin Christ, Germany).

2.6. Fluorescence staining

The binding of the fluorescently labeled peptide RD2-c488 was tested on 20 μm cryo sections from the cortex of an AD patient. Room tempered sections were fixed in 4% formaldehyde in Tris-buffered saline (TBS) for 2 min at room temperature and washed three times for 3 min in TBS-T (1% Triton X-100 in TBS). Sections were blocked in 3% normal goat serum (NGS) and 3% bovine serum albumin in TBS-T and consecutively incubated for 1 h with RD2-c488 (1:400) in TBS in a humid chamber. Sections were washed five times for 3 min in TBS.

Immunofluorescence staining against amyloid β was performed using the directly labeled antibody 6E10-Alexa594 (1:500, Bio Legend, San Diego, USA). Sections were incubated with the primary antibody in 1% BSA in TBS at 4 °C overnight in a humid chamber. In the following, sections were washed five times for 3 min in TBS. In order to quench unspecific autofluorescence, sections were incubated with TrueBlack solution (Biotium via Linaris, Dossenheim, Germany) according to the standard conditions for 2 min. Slices were rinsed twice in TBS and washed for another 5 min in TBS to be mounted in Fluoromount (Sigma-Aldrich, Taufkirchen, Germany) for further analysis.

2.7. Methoxy-X04 staining

Fluorescence staining with Methoxy-X04 was performed to stain fibrillar amyloid on frozen sections.

Frozen 20 μm brain sections were dried in ambient air for 15 min, immersion-fixed in 4% formaldehyde in phosphate-buffered saline (PBS) at RT for 10 min, and then washed in PBS for 10 min. Methoxy-X04 (Tocris/Bio-Techne, Germany) was dissolved at 0.01 mg/ml in PBS, and sections were stained for 30 min at RT. Sections were rinsed three times for 5 min in PBS before washing in an ascending alcohol series and mounting with DPX Mountant (Sigma-Aldrich, Darmstadt, Germany).

2.8. Microscopy

Sections were acquired with the use of a Zeiss SteREO Lumar V12 (Carl Zeiss AG, Oberkochen, Germany) microscope and the associated software (Zeiss AxioVision 6.4 RE), and a Leica LMD6000 microscope (Leica Microsystems GmbH, Wetzlar, Germany) and the associated software (LAS 4.0 software).

2.9. Radiosynthesis

[^{18}F]RD2-cFPy was synthesized by palladium-catalyzed S-arylation of RD2cys with [^{18}F]FIPy, as previously reported (Humpert et al., 2021). Briefly, [^{18}F]FIPy was prepared from 1-(5-iodopyridin-2-yl)−1,4-diazabicyclo[2.2.2]octan-1-ium triflate using the "minimalist approach" (Richarz et al., 2014) by passing an aqueous solution of [^{18}F]fluoride over a Waters QMA carb anion exchange cartridge, which was subsequently flushed with anhydrous methanol and then eluted with a solution of the labeling precursor in methanol. The solvent was removed in a stream of argon under reduced pressure, followed by the addition of DMSO and heating of the reaction mixture to 100 °C for 15 min. The conjugation was performed at room temperature using a mixture of acetonitrile and aqueous phosphate buffer (pH 7.4) as the solvent and Xantphos Pd G3 as the catalyst. To this end, [^{18}F]FIPy was either purified by HPLC and reacted with 300 nmol of the cysteine-modified peptide or purified by SPE and reacted with 3 μmol of the cysteine-modified peptide. Subsequent HPLC purification afforded the desired product, [^{18}F]RD2-cFPy, in RCYs of 40 ± 7% or 41 ± 5%, respectively.

2.10. In vitro autoradiography

Brain sections were thawed to ambient temperature and rinsed for 5 min in TBS buffer pre-incubation. Subsequently, slides were incubated for 60 min with 23.1 kBq/ml [^{18}F]RD2-cFPy in TBS at room temperature (200 μl per section, $n = 4$). A subset of sections was incubated with unlabeled RD2 peptide as a competitor with a concentration of either 1.3 μM or 700 μM to block all binding sites. The % occupancy of RD2 at each of the high or low affinity binding sites was calculated according to the law of mass action with the following formula:

$$\text{fractional occupancy} = \frac{[\text{Ligand}]}{[\text{Ligand}] + K_D}$$

Incubation with 1.3 μM RD2 corresponded to 150 x the K_D value of the high affinity binding site (8 nM), about 15 x that of the binding site on oligomers (88 nM), and about 4 x that of the low affinity binding site on Aβ. Following the main incubation, slides were washed twice by dipping in ddH_2O and were dried in the incubator at 37 °C for 30 min. After the sections were completely dried, exposition against BAS-plates (Fuji BAS-SR2025, Fuji Photo Film Co., Ltd., Japan) for 60 min was performed. BAS-plates were scanned with the Fujifilm BAS-reader 5000 and analyzed with AIDA Image Analyzer 5.1 (Raytest Isotopenmeßgeräte GmbH, Straubenhardt, Germany).

2.11. Small animal PET

Dynamic [^{18}F]RD2-cFPy PET was acquired using an INVEON small animal PET-CT scanner (Siemens Preclinical Solutions Inc. Knoxville, TN, USA) with four ARTE10 animals aged 24 months and five age-matched C57Bl/6 wild-type control mice. After a 10 min transmission scan using a Co-57 point source for attenuation correction, animals received a slow (1 min) intravenous bolus injection of (mean +/- SD) 12.3 +/- 1.7 MBq [^{18}F]RD2-cFPy (specific activity: 22.6 +/- 7.5 GBq/μmol) in 150 μl saline under isoflurane anesthesia into the lateral tail vein using a tailor-made catheter. Dynamic data acquisition was performed in 3D listmode (1.51 × 1.51 × 10 mm lutetium oxyorthosilicate crystal elements; 16.1 cm ring diameter; 10 cm transaxial field of view (FOV); 12.7 cm axial FOV) for 90 min starting immediately with the injection of the tracer. The emission data were corrected for dead time, and sinograms were reconstructed with OSEM 3D into the 35 frames (10 × 5 s, 4 × 10 s, 5 × 30 s, 6 × 60 s, 4 × 300 s, 6 × 600 s), resulting in 159 slices with an image voxel size of 0.7764 × 0.7764 × 0.796 mm^3 (matrix size: 128 × 128 × 159). During reconstruction, images were normalized on a calibrated Ge-68 cylinder source to correct for detector inhomogeneities and count rate variability. Furthermore, images were corrected for attenuation and decay. For anatomical co-registration,

animals received a CT scan of 10 min immediately after the PET measurement. Following the CT scan, the deeply anesthetized mice were killed as described above.

2.12. PET data analysis

Data received from the PET scans were processed and analyzed with the PMOD 4.1 software package (Pmod Technologies, Zürich, Switzerland). The biodistribution of [^{18}F]RD2-cFPy was analyzed in whole-body scans of wild-type mice. Circular volumes of interest (VOIs) were defined for each of the following organs with the help of the maximal intensity projection function: heart, lungs, liver, one kidney, and brain. Time-activity curves (TACs) were calculated in each VOI based on the percentage of injected dose per tissue volume (%ID/ml). [^{18}F]RD2-cFPy distribution in each VOI was calculated for frames 16, 25, and 35, corresponding to 2, 10, and 85 min p.i., respectively. The distribution of [^{18}F]RD2-cFPy in the brains of APP/PS1 and wild-type mice was analyzed as described previously (Willuweit et al., 2021). Briefly, co-registration of individual CT images was performed to PMOD's magnetic resonance imaging (MRI) brain template, and manual rigid-body alignment was accomplished by co-registering [^{18}F]RD2-cFPy images from early frames (1.3 to 9.3 min p.i.) to the corresponding individual CT images. The resulting co-registration of the PET images to the MRI template was checked for quality control. Predefined VOIs from the MRI template were transformed back to the original dynamic PET images, and TACs were calculated in each VOI based on the percentage of injected dose per tissue volume (%ID/ml). VOIs were further analyzed in averaged frames from 10 to 90 min p.i..

2.13. Statistical analysis

All statistical analyses were performed using GraphPad Prism 8 (GraphPad Software, Inc., La Jolla, USA). The Gaussian distribution of all data was tested using the normality plot in GraphPad Prism. Normally distributed data were analyzed using the repeated measures two-way analysis of variance (ANOVA) using genotype and brain region as the main factors. Genotype was analyzed with two levels, and brain region was analyzed with seven levels. Sidak's post hoc analysis was performed by comparing each brain region of the wild-type mice with that of the transgenic animals. No multiple comparison test was performed to compare the brain regions. All data are presented as mean ± SEM or SD. P-values smaller than 0.05 were considered to indicate significant statistical differences.

3. Results

3.1. Design and synthesis of [^{18}F]RD2-cFPy

A common approach for the indirect radiolabeling of peptides is acylation of either the N-terminus or the side chain amino group of lysine residues with N-succinimidyl-4-[^{18}F]fluorobenzoate ([^{18}F]SFB). Although this method affords many labeled conjugates in good radiochemical yields (RCYs), preliminary studies with the lysine-modified lead compound D3 (D3-lys) furnished no product (Cavani, 2015), which is in agreement with previous reports of low RCYs for coupling of [^{18}F]SFB to peptides containing multiple arginine residues (Tang et al., 2010; Kuchar et al., 2012). As an alternative radiolabeling strategy, we examined maleimide-thiol coupling with the prosthetic group 1-[3-(2-[^{18}F]fluoropyridine-3-yloxy)propyl]pyrrole-2,5-dione ([^{18}F]FPyME). However, while the conjugation of [^{18}F]FPyME to D-cysteine-modified D3 (D3-cys) was nearly quantitative, non-decay corrected yields for the prosthetic group itself did not exceed 25%, even after optimizing the synthetic route with regard to reaction steps and synthesis time (Cavani et al., 2017). Due to the long overall synthesis time of 120 min, yields of the labeled D3 derivative were also concomitantly low. With this in mind, we reasoned that radiolabeling of RD2 using our recently reported, highly efficient thiol-coupling using palladium-catalyzed S-arylation with 2-[^{18}F]fluoro-5-iodopyridine ([^{18}F]FIPy) could give considerably higher overall yields (Humpert et al., 2021). [^{18}F]FIPy can be rapidly synthesized in excellent RCYs of 70–80%, requires no HPLC purification if the concentration of thiol-containing substrate is sufficiently high, and can be conjugated to suitable substrates in RCYs of up to 70% within only 6 min. Thus, using cysteine-modified RD2-cys, we were able to synthesize the radiolabeled RD2 derivative [^{18}F]RD2-cFPy (Fig. 1) in about 40% of overall RCY within 60 min, as described in more detail in Section 2.9.

3.2. Binding of [^{18}F]RD2-cFPy to brain sections from transgenic mice and AD patients

Specific binding of [^{18}F]RD2-cFPy to the brains of an APP/PS1 transgenic mouse model (ARTE10) was confirmed by *in vitro* autoradiography. The ARTE10 line is a homozygous amyloidosis model, which develops a robust and progressive AD-like plaque pathology in the brain and has already proven itself in preclinical imaging studies (Willuweit et al., 2009, 2021). High binding of [^{18}F]RD2-cFPy was found in brain regions with high amyloid loads, such as the cortex and the hippocampus (Fig. 2A, B), but was not found in the brain of an age-matched control mouse (Fig. 2C). Competition with unlabeled RD2 was able to completely block [^{18}F]RD2-cFPy binding to the APP/PS1 brain (Fig. 2D).

Likewise, [^{18}F]RD2-cFPy showed high binding to cortical tissue in a human AD subject (Fig. 3A). In terms of the binding of RD2 to monomeric Aβ, low and high affinity binding has been described with K_D values of 8 nM and 330 nM, respectively (Zhang et al., 2019). In addition, we determined the binding affinity to monomeric subunits in Aβ oligomers with a K_D value of about 88 nM and to Aβ fibrils with a K_D of 4 μM (Fig. S1). By adding 1.3 μM unlabeled RD2 as a competitor in the experiment, the 8 nM and 88 nM binding sites were blocked to 99.3% and 93.75%, respectively, while the low affinity binding site was blocked by about 80%. Therefore, residual binding of [^{18}F]RD2-cFPy to the cortical section in the presence of 1.3 μM RD2 mainly represents the binding of the radioligand to the low affinity binding site (about 20%, Fig. 3B), while increasing the competitor concentration to 700 μM RD2 blocks all specific [^{18}F]RD2-cFPy binding completely, including the binding to A**β** fibrils (Fig. 3C). Control tissue with minimal amounts of Aβ oligomers was taken from the cerebellum of a healthy 64-year-old. Although it can be assumed that the cortex of the healthy 64-year-old control subject will already contain certain amounts of soluble Aβ assemblies, the Aβ levels in the cerebellum would be expected to be very low. In comparison to the cortex of the AD subject, binding to the cerebellum control showed lower [^{18}F]RD2-cFPy binding, which could mainly be competed from the low affinity binding site with high competitor concentrations (Fig. 3D to F). For the quantification of the *in vitro* autoradiography, please refer to Fig. 4. As expected from the cerebral Aβ load of old individuals over the age of 80, the binding of [^{18}F]RD2-cFPy to the cortex of age-matched, non-demented subjects (Braak stage 2, see Table S1) was somewhat lower, although still substantial, than the binding to the AD cortex (Fig. S2).

3.3. Localization of RD2 on brain sections

The D-enantiomeric peptide RD2 was designed to bind to Aβ monomers and, thus, also to Aβ subunits in oligomers and larger aggregates. In order to visualize its binding abilities, RD2 was labeled with a fluorescent dye, yielding RD2-c488. Cryo sections of the cortex of an AD patient were incubated with RD2-c488, and double staining with an antibody against human Aβ demonstrated co-localization of RD2-c488 with amyloid deposits (Fig. 5).

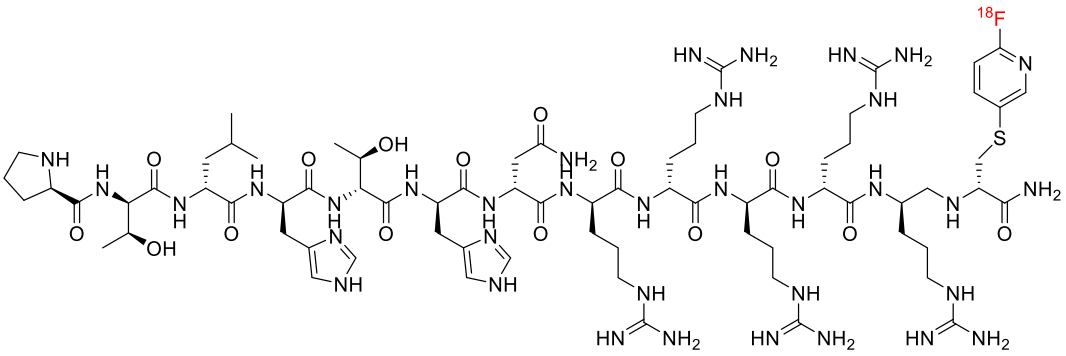

H-pro-thr-leu-his-thr-his-asn-arg-arg-arg-arg-arg-cys([^{18}F]FPy)-NH_2

Fig. 1. Lewis structure of [^{18}F]RD2-cFPy.

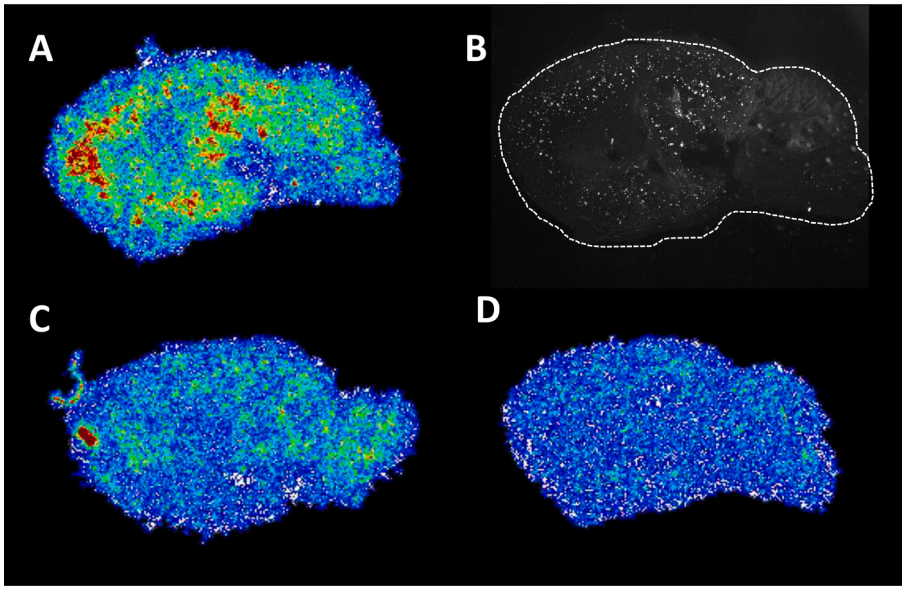

Fig. 2. Binding of [^{18}F]RD2-cFPy to Aβ present in the brain of transgenic mice. *In vitro* autoradiography with [^{18}F]RD2-cFPy on sagittal brain sections of an APP/PS1 transgenic (A, D) or an age-matched wild-type mouse (C). Competition with 700 μM unlabeled RD2 blocks binding of [^{18}F]RD2-cFPy to the APP/PS1 brain (D). Localization of amyloid in the brain of the APP/PS1 mouse is shown by Methoxy-X04 staining (B).

3.4. Biodistribution of [^{18}F]RD2-cFPy

In order to measure the biodistribution of [^{18}F]RD2-cFPy *in vivo,* the radioligand was injected IV into wild-type mice and uptake into several organs was measured using dynamic PET analysis. During the early phase following injection, [^{18}F]RD2-cFPy mainly distributed into the heart, kidneys, liver and lungs (Table 1). Thereafter, the radioligand was washed out of the heart and lungs, but distribution into the liver, and especially the kidneys, increased over time. Uptake into the brain was much lower and showed slightly longer wash-out over time compared to the heart and lungs.

3.5. Distribution of [^{18}F]RD2-cFPy in the brains of wild-type and APP/PS1 mice

Uptake of [^{18}F]RD2-cFPy into the brain was analyzed in more detail by comparing wild-type and transgenic APP/PS1 mice. Averaged time-activity curves in volumes-of-interest (VOIs) covering the whole brain reached a maximal concentration of around 1% ID/ml in the brains of transgenic animals and decreased over time towards values around 0.4% ID/ml. Furthermore, time-activity curves showed a tendency of more [^{18}F]RD2-cFPy retention in APP/PS1 transgenic *versus* wild-type mice (Fig. 6A). This tendency was confirmed when individual brain areas were analyzed in averaged frames from 10 to 90 min p.i. and was most obvious in the cortical VOI (Fig. 6B). However, due to one transgenic animal with very low cortical uptake, the data missed statistical significance (two-way-ANOVA: main factor brain region, $F(2.102, 14.72) = 85.73$, $p < 0.0001$; main factor genotype, $F(1, 7) = 0.5112$, $p = 0.498$; brain region x genotype, $F(6, 42) = 1.617$, $p = 0.166$).

4. Discussion

The aim of the current study is the design and evaluation of a novel amyloid PET probe based on a D-enantiomeric peptide. One of the most obvious advantages of D-peptides is their high stability in bodily fluids, such as blood (Elfgen et al., 2019, 2017). Since endogenous proteases are selective for L-peptides, D-peptides are not degraded or are degraded very slowly. Thus, D-peptides combine the high specificity of peptides with high proteolytic stability. In addition, D-peptides are virtually non-immunogenic (Dintzis et al., 1993). Given these advantages, D-peptides are assumed to be suitable for the development of targeted PET probes.

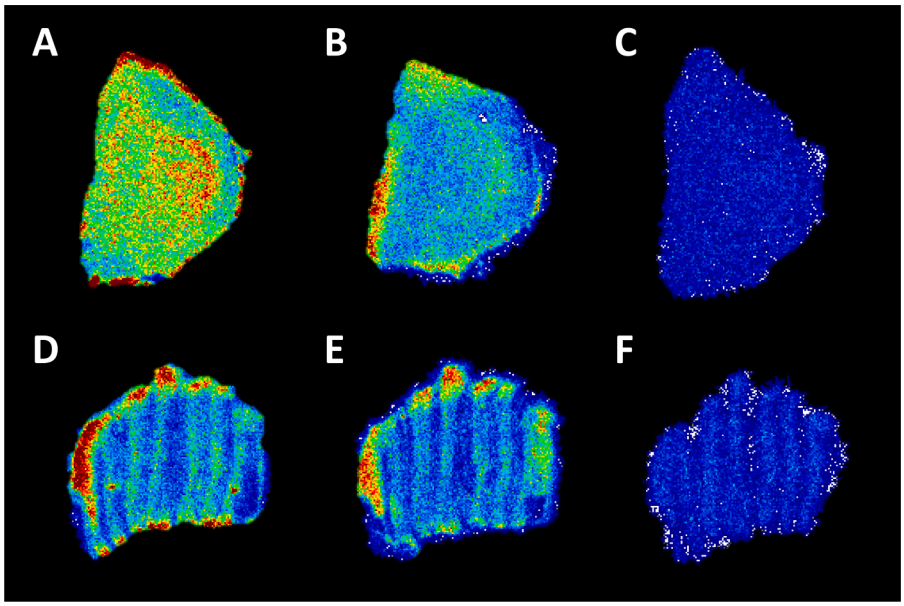

Fig. 3. Binding and competition of [^{18}F]RD2-cFPy in human brain sections. *In vitro* autoradiography with [^{18}F]RD2-cFPy on cryo sections from the cortex of an AD patient (A–C) or cerebellum of a control subject (D–F). [^{18}F]RD2-cFPy exhibits more binding to the AD brain (A) than to the control (D). Incubation with 1.3 μM (B, E) or with 700 μM (C, F) unlabeled RD2 competes with high and low affinity binding of [^{18}F]RD2-cFPy, respectively. Of note, artifacts resulting from cutting the tissue caused striped binding patterns and higher binding at the rim of the sections.

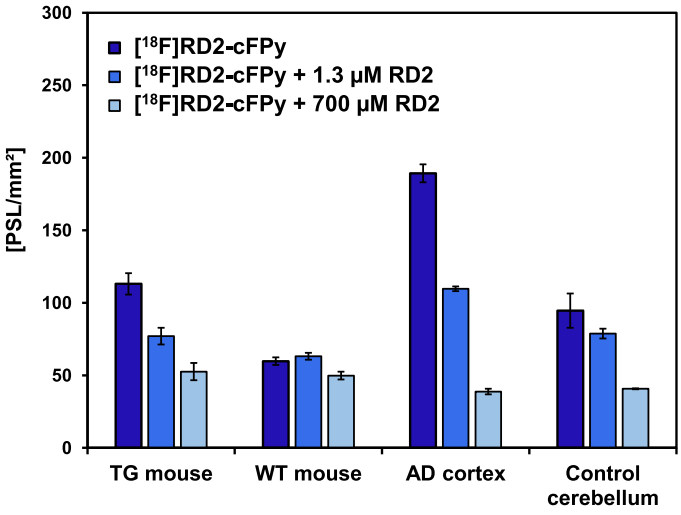

Fig. 4. Quantification of *in vitro* autoradiography with [^{18}F]RD2-cFPy. Binding of [^{18}F]-RD2-cFPy to human brain sections (AD or control) from the cortex or cerebellum, and to the cortex of APP/PS1 transgenic (TG) or wild-type (WT) mice was quantified after exposure to phosphoimaging plates. Competition binding was quantified after the addition of either 1.3 μM or 700 μM unlabeled RD2. Data are presented as mean +/- SD of three to four brain sections. PSL, photostimulated luminescence.

Here, we tested this hypothesis using the D-enantiomeric dodecapeptide RD2. The all-D-peptide RD2 was designed to destabilize and disassemble Aβ oligomers and other Aβ assemblies as a therapeutic strategy against AD. RD2 was shown to penetrate the brain (Leithold et al., 2016) and bind to monomeric Aβ subunits in oligomers and larger aggregates, which leads to the disassembly of the Aβ complexes (Schemmert et al., 2019b; Kass et al., 2022; Brener et al., 2015). Proof of concept for this therapeutic strategy has been shown in various animal models of AD (van Groen et al., 2017; Kutzsche et al., 2017; Schemmert et al., 2019a, 2019b; Kutzsche et al., unpublished results). RD2 has been demonstrated to be very stable in bodily fluids, such as simulated gastric and intestinal fluid and blood. A half-life of 216 h has been determined in human plasma in comparison to a half-life of 2 h for the corresponding L-enantiomer of RD2. Furthermore, after incubation with human liver microsomes, 66.6% of RD2 was still intact after 24 h, while the L-enantiomer was almost completely degraded within 30 min. (Elfgen et al., 2019).

We radiolabeled the RD2 peptide after introducing an additional D-cysteine residue at the C-terminus using palladium-catalyzed S-arylation with 2-[^{18}F]Fluoro-5-iodopyridine ([^{18}F]FIPy). The specificity of the resulting radiolabeled compound, [^{18}F]RD2-cFPy, for targeting Aβ was evaluated using brain sections from APP/PS1 transgenic *versus* wild-type mice and material from the cortex of AD patients. The binding of [^{18}F]RD2-cFPy was demonstrated in brain areas with high amyloid load, such as the cortex of APP/PS1 transgenic mice, which can be expected to contain not only fibrillary but also oligomeric Aβ. Co-localization of RD2 with amyloid plaques in the cortex of an AD patient was also confirmed with higher resolution using fluorescently-labeled RD2 and an antibody against Aβ. However, residual binding of [^{18}F]RD2-cFPy was also found in brain sections of wild-type mice and the cerebellum of a control subject, which was assumed to contain only very small amounts of Aβ oligomers. Since Aβ is produced throughout a lifetime, the initial formation of oligomeric assemblies in a control subject of 64 years cannot be excluded. For this reason, the cerebellum was chosen as control tissue as amyloid pathology here is normally very scarce. However, competition binding experiments identified residual binding to the control tissue as low affinity binding. For the interaction between RD2 and Aβ, high and low affinity binding was demonstrated with K_D values of 8 and 330 nM, respectively (Zhang et al., 2019). In principle, one could also assume these binding sites to be present on Aβ subunits within oligomeric and higher molecular weight assemblies. Here, we additionally determined the binding affinities of RD2 to *in vitro* assembled Aβ oligomers and fibrils with a K_D of 88 nM and 4 μM, respectively. These results indicate that RD2 has a clear preference towards binding to soluble Aβ species. That being said, the affinity of RD2 to Aβ oligomers was determined to be tenfold lower than that of Aβ monomers, which might reflect structural changes of Aβ within the oligomeric complex, resulting in lower binding to RD2. However, the actual binding of a ligand to its binding partner is not only determined by the binding affinity but also by the concentrations of the binding partners. Since oligomers and larger aggregates have a very high local concentration of Aβ subunits and, thus, potential binding sites, high sequestration of RD2 can be assumed, increasing binding avidity. The co-localization of fluorescently-labeled RD2 with amyloid plaques on brain slices of AD patients despite the low binding affinity to Aβ fibrils supports this hypothesis. Therefore, based on current data, it can be assumed that [^{18}F]RD2-cFPy does preferentially bind to soluble Aβ aggregates over fibrillar Aβ aggregates.

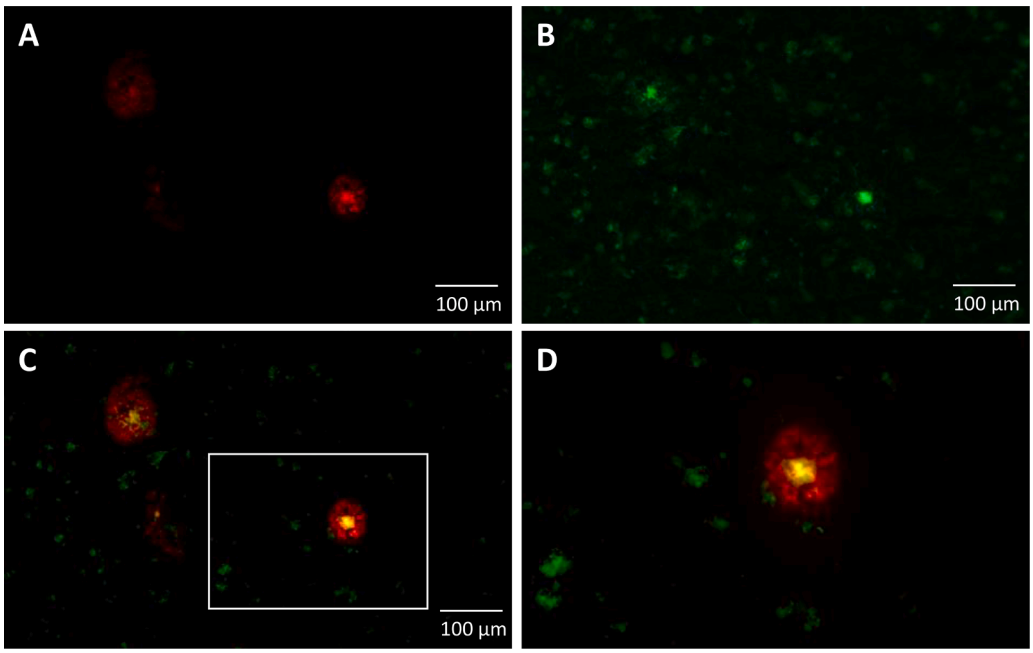

Fig. 5. Co-localization of fluorescently labeled RD2 with Aβ. Cryo sections from the cortex of an AD patient were immuno-stained with an antibody against Aβ (6E10, A) and incubated with fluorescently-labeled RD2, termed RD2-c488 (B). Overlay images show co-localization mainly in the core of amyloid plaques (C, D). (D) is a magnification of the inset shown in (C).

Table 1
Biodistribution of [^{18}F]RD2-cFPy in wild-type mice at several times post injection (p.i.). Data is quantified from *in vivo* PET measurement and is presented as mean +/- SEM from $n = 5$ animals.

Time p.i. [min]	Heart [%ID/ml] [1]	Kidney [%ID/ml]	Liver [%ID/ml]	Lungs [%ID/ml]	Brain [%ID/ml]
2	10.59 +/- 1.17	15.30 +/-1.66	8.73 +/- 0.64	8.91 +/- 0.31	0.73 +/- 0.07
10	4.81 +/- 0.68	20.03 +/- 1.97	9.32 +/- 1.12	4.69 +/- 0.35	0.46 +/- 0.05
85	1.22 +/- 0.23 (11.5 +/- 2.2%)[2]	34.40 +/- 3.73 (224.8 +/- 24.4%)[2]	22.14 +/- 3.61 (254.6 +/- 41.4%)[2]	1.81 +/- 0.43 (20.3 +/- 4.8%)[2]	0.24 +/- 0.07 (32.9 +/- 9.6%)[2]

[1] %ID/ml,% injected dose per ml volume.
[2] values are given as quotient referenced to the initial values at 2 min p.i.

However, it does not seem able to completely discriminate between soluble oligomers and higher molecular weight assemblies, including large fibrils. In this respect, the amount of Aβ oligomers in the brains of AD patients is of importance. Recently, the levels of soluble Aβ oligomers within human brain homogenates have been quantified to be at least 100 pM in AD patients and around 2 pM in non-demented controls (Kass et al., 2022). In order to demonstrate the ability of the radioprobe to detect soluble oligomers without interference from insoluble aggregates, experiments with an animal model only harboring Aβ oligomers would be needed. The prerequisite for these kinds of experiments would be the thorough characterization of our animal model on the temporal development of Aβ oligomer levels in the brain and in comparison to the occurrence of larger insoluble aggregates.

Both the monomeric and oligomeric binding sites were competed by the addition of different concentrations of unlabeled RD2 to cortical tissue from an AD patient and APP/PS1 mice, while mainly low affinity binding was found in the control tissue. We assume that low affinity binding of RD2 to Aβ is mainly due to Coulomb interactions of the positively charged RD2 to the N-terminal amino acid residues of Aβ. This low affinity is not very specific and might be the cause of unspecific binding to negatively charged binding sites not only present in the cerebellum. Recently, it was shown that D3, the lead compound of RD2, dynamically interacts with membrane-bound Aβ precursors (Bocharov et al., 2021) with low affinity (K_D between 11 and 39 µM). Likewise, low affinity binding of RD2 to membrane-bound Aβ precursors may also partly explain binding to brain sections from the wild-type mice and to the cerebellum of the control subject.

The biodistribution of [^{18}F]RD2-cFPy in wild-type mice was investigated by means of *in vivo* PET analysis. Organs with a high initial uptake followed by fast wash-out kinetics included the heart and lungs, and it could be speculated that such kinetics might indicate initial binding of [^{18}F]RD2-cFPy to only the vasculature of the organs after IV administration but no penetration or retention in the tissue. In contrast, the increase of [^{18}F]RD2-cFPy over time in the liver and mainly in the kidneys indicates penetration, retention, and probably also the excretion of the radioprobe via these organs. For a tritium-labeled version of RD2, high concentrations in the kidneys were demonstrated after IV administration, and the kidneys were assumed to be the primary excretion organ in mice for this administration route (Leithold et al., 2016). Distribution of [^{18}F]RD2-cFPy into the brain was much lower and showed wash-out over time. The concentrations of [^{18}F]RD2-cFPy found in the whole brain after 85 min were comparable to that quantified using the tritium-labeled version of RD2 (Leithold et al., 2016).

A closer look at the uptake kinetics of [^{18}F]RD2-cFPy in the brain and its penetration into several brain regions was taken by comparing its retention in wild-type *versus* APP/PS1 transgenic mice. In fact, by analyzing the average retention over 10 to 90 min p.i in different brain regions, we were able to find a tendency of more [^{18}F]RD2-cFPy in the brains of transgenic mice. In particular, [^{18}F]RD2-cFPy reached higher concentrations in the cortex of the majority of transgenic mice. However, a hundred percent discrimination between the groups could not be reached with our experimental set-up and within the limited time frame of the PET scan. It would be interesting to see whether [^{18}F]RD2-cFPy is able to clearly discriminate between wild-type and transgenic mice after a prolonged wash-out period of several hours or days. This, however, is not possible with the radionuclide chosen here and would require labeling with longer-lived positron-emitting radionuclides, such as ^{124}I or ^{89}Zr (half-life of 4.2 d and 3.3 d, respectively), which are frequently used

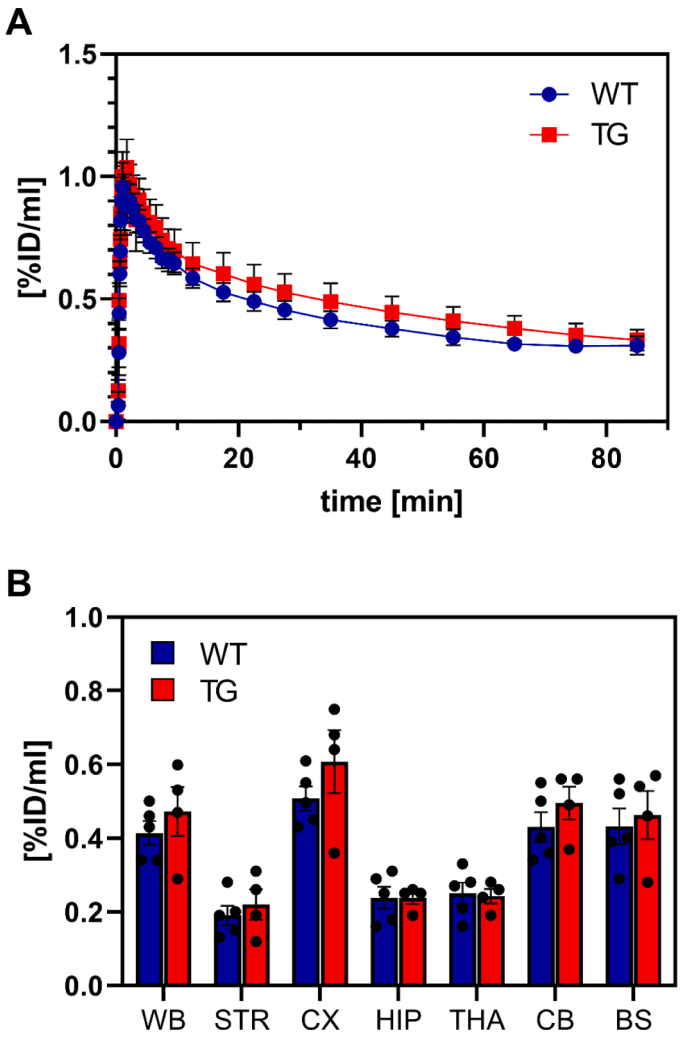

Fig. 6. PET analysis of the brain using [^{18}F]RD2-cFPy. Wild-type (WT, $n = 5$) or APP/PS1 transgenic (TG, $n = 4$) mice received a bolus IV injection of [^{18}F]RD2-cFPy and were subjected to PET analysis. **A**, Time-activity curves of [^{18}F]RD2-cFPy retention in the whole brain expressed as % injected dose (%ID) per ml tissue. **B**, Average distribution of [^{18}F]RD2-cFPy into the whole brain (WB) or different brain areas was analyzed 10 to 90 min p.i. Data are presented as mean +/- SEM. Each symbol represents data from one individual. BS, brain stem; CB, cerebellum; CX, cortex; HIP, hippocampus; STR, striatum; THA, thalamus; WB, whole brain.

for antibody-based radiotracers (Sehlin et al., 2019), or with a pre-targeted imaging approach (Krishnan et al., 2017).

Although the brain penetration of [^{18}F]RD2-cFPy appeared to be rather low, reaching a maximal concentration (c_{max}) of around 1% injected dose per ml (%ID/ml), it is actually somewhat higher than that of described antibody tracers against Aβ. For radioprobes based on antibodies or Fab fragments c_{max}, values as low as 0.05 to 0.1% ID/g in brain tissue were reported (Sehlin et al., 2016; Magnusson et al., 2013). Coupling to an antibody binding the transferrin receptor has been shown to improve brain uptake of antibody probes (Sehlin et al., 2016). A range of different strategies for the optimization of cell- and brain-penetration of peptides exist, including the addition of known advantageous sequence motifs (Rockendorf et al., 2022). RD2 and its lead compound, D3, belong to a class of arginine-rich peptides, which are often described as being membrane permeable (Futaki, 2005). Indeed, D3 has been described to contain a sequence homology to the arginine-rich motif of the immunodeficiency virus type 1 (HIV-1) transactivator of transcription (Tat) protein (Jiang et al., 2016). HIV-1 Tat possesses well-known membrane permeating properties via an adsorptive-mediated mechanism by binding to negatively charged targets like heparane sulfate/glycosaminoglycans or phospholipids on the membrane surface and through a passive uptake mechanism. For D3 and RD2 the same passive transport through the blood-brain-barrier via an adsorptive-mediated transcytosis mechanism was proposed (Jiang et al., 2016; Liu et al., 2010).

In addition to the long wash-out kinetics of [^{18}F]RD2-cFPy, a second reason for missing discrimination of Aβ content between wild-type and APP/PS1 transgenic mice might be residual binding to monomeric Aβ. Although RD2 can be assumed to show more binding to Aβ oligomers and larger aggregates, as pointed out above, it could still bind to murine monomeric Aβ, which is present in the brains of wild-type mice. However, the *in vitro* autoradiography results suggest that this is only a very small portion (Fig. 3). RD2 was optimized to bind and disassemble all kinds of oligomeric or larger Aβ assemblies by binding to the Aβ subunits and forcing them into the physiological monomeric conformation (Zhang et al., 2019; Kass et al., 2022). The attractiveness of this strategy is that RD2 can bind to all polymorphic oligomer variants and possible Aβ prion strains, including N-terminally truncated and modified Aβ. This is an advantage over antibody-based strategies, which are developed against a particular Aβ assembly and are very specific to their particular epitope and, thus, to a particular polymorph. Nevertheless, while RD2's described mechanism of action works very well for therapeutic purposes, RD2 has not been optimized as a diagnostic agent. Therefore, there is much room for the optimization of RD2 and the development of an improved D-enantiomeric peptidic radioprobe directed against Aβ.

In conclusion, this pilot study provides *in vivo* proof of concept for a radiotracer based on a D-enantiomeric peptide binding to Aβ. To the best of our knowledge; this is the first demonstration of *in vivo* PET analysis using a ^{18}F-labeled all D-peptide and could be the foundation for a new class of PET imaging agents in the future.

CRediT authorship contribution statement

Antje Willuweit: Conceptualization, Formal analysis, Data curation, Writing – original draft, Supervision, Project administration, Funding acquisition. **Swen Humpert:** Methodology, Investigation. **Michael Schöneck:** Formal analysis, Investigation, Visualization. **Heike Endepols:** Formal analysis, Writing – review & editing, Supervision. **Nicole Burda:** Investigation, Visualization. **Lothar Gremer:** Methodology, Investigation, Writing – review & editing, Supervision. **Ian Gering:** Methodology, Investigation. **Janine Kutzsche:** Supervision. **N.Jon Shah:** Funding acquisition. **Karl-Josef Langen:** Conceptualization, Supervision, Funding acquisition. **Bernd Neumaier:** Conceptualization, Methodology, Writing – review & editing, Supervision, Funding acquisition. **Dieter Willbold:** Conceptualization, Writing – review & editing, Supervision, Funding acquisition. **Alexander Drzezga:** Conceptualization, Writing – review & editing, Supervision, Funding acquisition.

Declaration of Competing Interest

A.W. and D.W. are co-founders of Priavoid GmbH, Düsseldorf, Germany. A.W. is a part-time employee, and D.W. is a member of the supervisory board of Priavoid, which develops RD2 as a therapeutic compound. Priavoid holds no intellectual property concerning the development of RD2 as a diagnostic compound. All other authors declare no conflict of interest.

Data availability

Data will be made available on request.

Institutional review board statement

The study was conducted in accordance with the Declaration of

Helsinki, and approved by the Ethics Committee of Heinrich Heine University Duesseldorf (Germany, study ID: 2018–115-FmB). The animal study protocol was approved by the Institutional Review Board responsible for Forschungszentrum Jülich (Landesamt für Natur, Umwelt und Verbraucherschutz Nordrhein-Westfalen (LANUV), North-Rhine-Westphalia, Germany, Az 84–02.04.2014.A362, Az 84–02.04.2017.A029 and Az 81–02.04.2019.A304).

Informed consent statement

The Netherlands Brain Bank obtained informed consent from all subjects involved in the study.

Acknowledgments

We thank Taconic Biosciences for kindly providing the ARTE10 mice. The authors wish to thank Saskia Bremen and Florian Schmitz for excellent technical support, along with Nikola Kornadt-Beck and all the care takers at the animal house for their support and care for the animals, and Claire Rick for improving the language of the manuscript. Publications fees were funded by the Deutsche Forschungsgemeinschaft (DFG, German Research Foundation) – 491111487.

Supplementary materials

Supplementary material associated with this article can be found, in the online version, at doi:10.1016/j.ejps.2023.106421.

References

Aileen Funke, S., van Groen, T., Kadish, I., Bartnik, D., Nagel-Steger, L., Brener, O., Sehl, T., Batra-Safferling, R., Moriscot, C., Schoehn, G.;, et al., 2010. Oral treatment with the D-enantiomeric peptide D3 improves the pathology and behavior of Alzheimer's disease transgenic mice. ACS Chem. Neurosci. 1, 639–648. https://doi.org/10.1021/cn100057j.

Bocharov, E.V., Gremer, L., Urban, A.S., Okhrimenko, I.S., Volynsky, P.E., Nadezhdin, K. D., Bocharova, O.V., Kornilov, D.A., Zagryadskaya, Y.A., Kamynina, A.V., et al., 2021. All-D-enantiomeric peptide D3 designed for Alzheimer's disease treatment dynamically interacts with membrane-bound amyloid-beta precursors. J. Med. Chem. 64, 16464–16479. https://doi.org/10.1021/acs.jmedchem.1c00632.

Brener, O., Dunkelmann, T., Gremer, L., van Groen, T., Mirecka, E.A., Kadish, I., Willuweit, A., Kutzsche, J., Jurgens, D., Rudolph, S., et al., 2015. QIAD assay for quantitating a compound's efficacy in elimination of toxic Abeta oligomers. Sci. Rep. 5, 13222. https://doi.org/10.1038/srep13222.

Cavani, M., Bier, D., Holschbach, M., Coenen, H.H., 2017. Efficient synthesis of [(18) F] FPyME: a new approach for the preparation of maleimide-containing prosthetic groups for the conjugation with thiols. J. Labelled Comp. Radiopharm. 60, 87–92. https://doi.org/10.1002/jlcr.3469.

Cavani, M., 2015. 18F-Markierung Hochaffiner All-D-Peptide Zur *in Vivo* Diagnostik von b-Amyloid-Plaques. University of Cologne, Cologne, Germany. PhD ThesisJune. http://hdl.handle.net/2128/9007.

Cohen, A.D., Rabinovici, G.D., Mathis, C.A., Jagust, W.J., Klunk, W.E., Ikonomovic, M.D., 2012. Using Pittsburgh compound B for *in vivo* PET imaging of fibrillar amyloid-beta. Adv. Pharmacol. 64, 27–81. https://doi.org/10.1016/B978-0-12-394816-8.00002-7.

Dintzis, H.M., Symer, D.E., Dintzis, R.Z., Zawadzke, L.E., Berg, J.M., 1993. A comparison of the immunogenicity of a pair of enantiomeric proteins. Proteins 16, 306–308. https://doi.org/10.1002/prot.340160309.

Dubois, B., Feldman, H.H., Jacova, C., Dekosky, S.T., Barberger-Gateau, P., Cummings, J., Delacourte, A., Galasko, D., Gauthier, S., Jicha, G., et al., 2007. Research criteria for the diagnosis of Alzheimer's disease: revising the NINCDS-ADRDA criteria. Lancet Neurol. 6, 734–746. https://doi.org/10.1016/S1474-4422(07)70178-3.

Elfgen, A., Santiago-Schubel, B., Gremer, L., Kutzsche, J., Willbold, D., 2017. Surprisingly high stability of the Abeta oligomer eliminating all-D-enantiomeric peptide D3 in media simulating the route of orally administered drugs. Eur. J. Pharm. Sci. 107, 203–207. https://doi.org/10.1016/j.ejps.2017.07.015.

Elfgen, A., Hupert, M., Bochinsky, K., Tusche, M., Gonzalez de San Roman Martin, E., Gering, I., Sacchi, S., Pollegioni, L., Huesgen, P.F., Hartmann, R., et al., 2019. Metabolic resistance of the D-peptide RD2 developed for direct elimination of amyloid-beta oligomers. Sci. Rep. 9, 5715. https://doi.org/10.1038/s41598-019-41993-6.

Funke, S.A., Willbold, D., 2009. Mirror image phage display–a method to generate D-peptide ligands for use in diagnostic or therapeutical applications. Mol. Biosyst. 5, 783–786. https://doi.org/10.1039/b904138a.

Futaki, S., 2005. Membrane-permeable arginine-rich peptides and the translocation mechanisms. Adv. Drug. Deliv. Rev. 57, 547–558. https://doi.org/10.1016/j.addr.2004.10.009.

Humpert, S., Omrane, M.A., Urusova, E.A., Gremer, L., Willbold, D., Endepols, H., Krasikova, R.N., Neumaier, B., Zlatopolskiy, B.D., 2021. Rapid (18)F-labeling via Pd-catalyzed S-arylation in aqueous medium. Chem. Commun. (Camb.) 57, 3547–3550. https://doi.org/10.1039/d1cc00745a.

Jack Jr., C.R., Wiste, H.J., Lesnick, T.G., Weigand, S.D., Knopman, D.S., Vemuri, P., Pankratz, V.S., Senjem, M.L., Gunter, J.L., Mielke, M.M., et al., 2013. Brain beta-amyloid load approaches a plateau. Neurology 80, 890–896. https://doi.org/10.1212/WNL.0b013e3182840bbe.

Jiang, N., Frenzel, D., Schartmann, E., van Groen, T., Kadish, I., Shah, N.J., Langen, K.J., Willbold, D., Willuweit, A., 2016. Blood-brain barrier penetration of an Abeta-targeted, arginine-rich, D-enantiomeric peptide. Biochim. Biophys. Acta 1858, 2717–2724. https://doi.org/10.1016/j.bbamem.2016.07.002.

Kass, B., Schemmert, S., Zafiu, C., Pils, M., Bannach, O., Kutzsche, J., Bujnicki, T., Willbold, D., 2022. Abeta oligomer concentration in mouse and human brain and its drug-induced reduction *ex vivo*. Cell Rep. Med. 3, 100630 https://doi.org/10.1016/j.xcrm.2022.100630.

Krishnan, H.S., Ma, L., Vasdev, N., Liang, S.H., 2017. (18) F-labeling of sensitive biomolecules for positron emission tomography. Chemistry (Easton) 23, 15553–15577. https://doi.org/10.1002/chem.201701581.

Kuchar, M., Pretze, M., Kniess, T., Steinbach, J., Pietzsch, J., Loser, R., 2012. Site-selective radiolabeling of peptides by (18)F-fluorobenzoylation with (18F)SFB in solution and on solid phase: a comparative study. Amino Acids 43, 1431–1443. https://doi.org/10.1007/s00726-012-1216-z.

Kutzsche, J., Schemmert, S., Tusche, M., Neddens, J., Rabl, R., Jurgens, D., Brener, O., Willuweit, A., Hutter-Paier, B., Willbold, D., 2017. Large-scale oral treatment study with the four most promising D3-derivatives for the treatment of Alzheimer's disease. Molecules 22. https://doi.org/10.3390/molecules22101693.

Kutzsche, J., Jurgens, D., Willuweit, A., Adermann, K., Fuchs, C., Simons, S., Windisch, M., Humpel, M., Rossberg, W., Wolzt, M., et al., 2020. Safety and pharmacokinetics of the orally available antiprionic compound PRI-002: a single and multiple ascending dose phase I study. Alzheimers Dement (N Y) 6, e12001. https://doi.org/10.1002/trc2.12001.

Kutzsche, J., Schemmert, S., Bujnick, T., Zafiu, C., Halbgebauer, S., Kraemer-Schulien, V., Pils, M., Bl..meke, L., Post, J., Kulawik, A., et al., unpublished result. Beta-amyloid oligomer disassembly decreases tau oligomer concentration and enhances cognition and memory in aged Beagle dogs. .submitted.

Leithold, L.H., Jiang, N., Post, J., Ziehm, T., Schartmann, E., Kutzsche, J., Shah, N.J., Breitkreutz, J., Langen, K.J., Willuweit, A., et al., 2016. Pharmacokinetic properties of a novel D-peptide developed to be therapeutically active against toxic beta-amyloid oligomers. Pharm. Res. 33, 328–336. https://doi.org/10.1007/s11095-015-1791-2.

LeVine 3rd, H., Walker, L.C., 2016. What amyloid ligands can tell us about molecular polymorphism and disease. Neurobiol. Aging 42, 205–212. https://doi.org/10.1016/j.neurobiolaging.2016.03.019.

Liu, H., Funke, S.A., Willbold, D., 2010. Transport of Alzheimer disease amyloid-beta-binding D-amino acid peptides across an *in vitro* blood-brain barrier model. Rejuven. Res. 13, 210–213. https://doi.org/10.1089/rej.2009.0926.

Magnusson, K., Sehlin, D., Syvanen, S., Svedberg, M.M., Philipson, O., Soderberg, L., Tegerstedt, K., Holmquist, M., Gellerfors, P., Tolmachev, V., et al., 2013. Specific uptake of an amyloid-beta protofibril-binding antibody-tracer in AbetaPP transgenic mouse brain. J. Alzheimers Dis. 37, 29–40. https://doi.org/10.3233/JAD-130029.

Mallik, A., Drzezga, A., Minoshima, S., 2017. Clinical amyloid imaging. Semin. Nucl. Med. 47, 31–43. https://doi.org/10.1053/j.semnuclmed.2016.09.005.

McKhann, G., Drachman, D., Folstein, M., Katzman, R., Price, D., Stadlan, E.M., 1984. Clinical diagnosis of Alzheimer's disease: report of the NINCDS-ADRDA work group under the auspices of department of health and human services task force on Alzheimer's disease. Neurology 34, 939–944. https://doi.org/10.1212/wnl.34.7.939.

Richarz, R., Krapf, P., Zarrad, F., Urusova, E.A., Neumaier, B., Zlatopolskiy, B.D., 2014. Neither azeotropic drying, nor base nor other additives: a minimalist approach to (18)F-labeling. Org. Biomol. Chem. 12, 8094–8099. https://doi.org/10.1039/c4ob01336k.

Roberts, R.O., Aakre, J.A., Kremers, W.K., Vassilaki, M., Knopman, D.S., Mielke, M.M., Alhurani, R., Geda, Y.E., Machulda, M.M., Coloma, P., et al., 2018. Prevalence and outcomes of amyloid positivity among persons without dementia in a longitudinal, population-based setting. JAMA Neurol. 75, 970–979. https://doi.org/10.1001/jamaneurol.2018.0629.

Rockendorf, N., Nehls, C., Gutsmann, T., 2022. Design of membrane active peptides considering multi-objective optimization for biomedical application. Membranes (Basel) 12. https://doi.org/10.3390/membranes12020180.

Rowe, C.C., Ackerman, U., Browne, W., Mulligan, R., Pike, K.L., O'Keefe, G., Tochon-Danguy, H., Chan, G., Berlangieri, S.U., Jones, G., et al., 2008. Imaging of amyloid beta in Alzheimer's disease with 18F-BAY94-9172, a novel PET tracer: proof of mechanism. Lancet Neurol. 7, 129–135. https://doi.org/10.1016/S1474-4422(08)70001-2.

Schemmert, S., Schartmann, E., Honold, D., Zafiu, C., Ziehm, T., Langen, K.J., Shah, N.J., Kutzsche, J., Willuweit, A., Willbold, D., 2019a. Deceleration of the neurodegenerative phenotype in pyroglutamate-Abeta accumulating transgenic mice by oral treatment with the Abeta oligomer eliminating compound RD2. Neurobiol. Dis. 124, 36–45. https://doi.org/10.1016/j.nbd.2018.10.021.

Schemmert, S., Schartmann, E., Zafiu, C., Kass, B., Hartwig, S., Lehr, S., Bannach, O., Langen, K.J., Shah, N.J., Kutzsche, J., et al., 2019b. Abeta oligomer elimination restores cognition in transgenic Alzheimer's mice with full-blown pathology. Mol. Neurobiol. 56, 2211–2223. https://doi.org/10.1007/s12035-018-1209-3.

Scholl, M., Wall, A., Thordardottir, S., Ferreira, D., Bogdanovic, N., Langstrom, B., Almkvist, O., Graff, C., Nordberg, A., 2012. Low PiB PET retention in presence of

pathologic CSF biomarkers in Arctic APP mutation carriers. Neurology 79, 229–236. https://doi.org/10.1212/WNL.0b013e31825fdf18.

Sehlin, D., Fang, X.T., Cato, L., Antoni, G., Lannfelt, L., Syvanen, S., 2016. Antibody-based PET imaging of amyloid beta in mouse models of Alzheimer's disease. Nat. Commun. 7, 10759. https://doi.org/10.1038/ncomms10759.

Sehlin, D., Syvanen, S., faculty, M., 2019. Engineered antibodies: new possibilities for brain PET? Eur. J. Nucl. Med. Mol. Imaging 46, 2848–2858. https://doi.org/10.1007/s00259-019-04426-0.

Serdons, K., Terwinghe, C., Vermaelen, P., Van Laere, K., Kung, H., Mortelmans, L., Bormans, G., Verbruggen, A., 2009. Synthesis and evaluation of 18F-labeled 2-phenylbenzothiazoles as positron emission tomography imaging agents for amyloid plaques in Alzheimer's disease. J. Med. Chem. 52, 1428–1437. https://doi.org/10.1021/jm8013376.

Tang, G., Tang, X., Wang, X., 2010. A facile automated synthesis of N-succinimidyl 4-[18F]fluorobenzoate ([18F]SFB) for 18F-labeled cell-penetrating peptide as PET tracer. J. Labelled Comp. Radiopharm. 53, 543–547. https://doi.org/10.1002/jlcr.1758.

Tolar, M., Hey, J., Power, A., Abushakra, S., 2021. Neurotoxic soluble amyloid oligomers drive alzheimer's pathogenesis and represent a clinically validated target for slowing disease progression. Int. J. Mol. Sci. 22. https://doi.org/10.3390/ijms22126355.

Tomiyama, T., Nagata, T., Shimada, H., Teraoka, R., Fukushima, A., Kanemitsu, H., Takuma, H., Kuwano, R., Imagawa, M., Ataka, S., et al., 2008. A new amyloid beta variant favoring oligomerization in Alzheimer's-type dementia. Ann. Neurol. 63, 377–387. https://doi.org/10.1002/ana.21321.

van Groen, T., Kadish, I., Funke, S.A., Bartnik, D., Willbold, D., 2013. Treatment with D3 removes amyloid deposits, reduces inflammation, and improves cognition in aged AbetaPP/PS1 double transgenic mice. J. Alzheimers Dis. 34, 609–620. https://doi.org/10.3233/JAD-121792.

van Groen, T., Schemmert, S., Brener, O., Gremer, L., Ziehm, T., Tusche, M., Nagel-Steger, L., Kadish, I., Schartmann, E., Elfgen, A., et al., 2017. The Abeta oligomer eliminating D-enantiomeric peptide RD2 improves cognition without changing plaque pathology. Sci. Rep. 7, 16275. https://doi.org/10.1038/s41598-017-16565-1.

Villain, N., Chetelat, G., Grassiot, B., Bourgeat, P., Jones, G., Ellis, K.A., Ames, D., Martins, R.N., Eustache, F., Salvado, O., et al., 2012. Regional dynamics of amyloid-beta deposition in healthy elderly, mild cognitive impairment and Alzheimer's disease: a voxelwise PiB-PET longitudinal study. Brain 135, 2126–2139. https://doi.org/10.1093/brain/aws125.

Walsh, D.M., Selkoe, D.J., 2007. A beta oligomers - a decade of discovery. J. Neurochem. 101, 1172–1184. https://doi.org/10.1111/j.1471-4159.2006.04426.x.

Wiesehan, K., Willbold, D., 2003. Mirror-image phage display: aiming at the mirror. ChemBioChem 4, 811–815. https://doi.org/10.1002/cbic.200300570.

Willbold, D., Strodel, B., Schroder, G.F., Hoyer, W., Heise, H., 2021. Amyloid-type protein aggregation and prion-like properties of amyloids. Chem. Rev. 121, 8285–8307. https://doi.org/10.1021/acs.chemrev.1c00196.

Willuweit, A., Velden, J., Godemann, R., Manook, A., Jetzek, F., Tintrup, H., Kauselmann, G., Zevnik, B., Henriksen, G., Drzezga, A., et al., 2009. Early-onset and robust amyloid pathology in a new homozygous mouse model of Alzheimer's disease. PLoS One 4, e7931. https://doi.org/10.1371/journal.pone.0007931.

Willuweit, A., Schoneck, M., Schemmert, S., Lohmann, P., Bremen, S., Honold, D., Burda, N., Jiang, N., Beer, S., Ermert, J., et al., 2021. Comparison of the amyloid load in the brains of two transgenic Alzheimer's disease mouse models quantified by florbetaben positron emission tomography. Front. Neurosci. 15, 699926 https://doi.org/10.3389/fnins.2021.699926.

Wong, D.F., Rosenberg, P.B., Zhou, Y., Kumar, A., Raymont, V., Ravert, H.T., Dannals, R. F., Nandi, A., Brasic, J.R., Ye, W., et al., 2010. *In vivo* imaging of amyloid deposition in Alzheimer disease using the radioligand 18F-AV-45 (florbetapir [corrected] F 18). J. Nucl. Med. 51, 913–920. https://doi.org/10.2967/jnumed.109.069088.

Zhang, T., Gering, I., Kutzsche, J., Nagel-Steger, L., Willbold, D., 2019. Toward the mode of action of the clinical stage All-D-enantiomeric peptide RD2 on Abeta42 aggregation. ACS Chem. Neurosci. 10, 4800–4809. https://doi.org/10.1021/acschemneuro.9b00458.